Catalytic Ozonation for Phenol Removal over Cobalt-doped α-MnO_2 Catalyst: Performance and Mechanism

Jie Zhang
College of Environmental and Spatial Informatics, China University of Mining and Technology
Ben Dong
College of Environmentall and Spatial Informatics, China University of Mining and Technology
Ying Han (1711479317@qq.com)
College of Environmental and Spatial Informatics, China University of Mining and Technology
Xiaocui Zhan
Tonling Nonferrous Design&Research Institute Co
Sijie Ge
College of Environmental and Spatial Informatics, China University of Mining and Technology
Shilong He
College of Environmental and Spatial Informatics.China University of Mining and Techonology

Research Article

Keywords: Phenol, Catalytic Ozonation, Co Doping, α-MnO2, Advanced Oxidation Process, Catalyst Structure

Posted Date: January 31st, 2022

DOI: https://doi.org/10.21203/rs.3.rs-1194666/v1

Abstract

In this paper, Cobalt-doped α-MnO_2 (i.e., Co-α-MnO_2) were synthesized through hydrothermal method. Phenol was employed as targeted pollutants to investigate the catalytic ozonation performance of Co-α-MnO_2 in terms of catalytic ability and mechanism. Results showed that that Co doped on α-MnO_2 significantly improved the phenol removal increased to 97.47 % after 40 min, which was 16.46 %, 38.92 % higher than that of α-MnO_2 catalytic ozonation and single ozonation without catalyst. In order to investigate the effect of Co doping on the physicochemical properties of the catalysts, the synthesized α-MnO_2 and Co-α-MnO_2 (2% Co/Mn doping ratio) catalysts were characterized by XRD, TEM, BET and XPS techniques, including the phase, morphology, structural properties and dispersity of the surface active species. The larger specific surface area and pore volume, more crystal defect and oxygen vacancy, higher relative content of Mn^{3+} and adsorbed oxygen (O_{ads}) as well as surface hydroxyl were obtained after Co doping on α-MnO_2, which could result in higher catalytic oxidation performance of Co-α-MnO_2. The influence of masking agent showed that surface hydroxyl group and active free radicals (•OH and $•O^{2-}$) were involved in the catalytic ozonation of phenol. This study could help recognize the role of surface hydroxyl groups and active free radicals and demonstrate the contribution of reactive oxygen species (ROS) on phenol removal in Co-α-MnO_2 systems.

1. Introduction

Ozonation has been widely undertaken in industrial wastewater treatment because ozone poses the outstanding oxidation potential on a large number of organic pollutants (Chen et al., 2017; Wang and Chen, 2020). However, single ozonation commonly presented a low removal rate on organic compounds degradation (Hu and Xia, 2018). To overcome the limitation of this process, ozonation coupled with catalyst have been attracted much attention. Heterogeneous catalytic ozonation can enhance the oxidation of ozone by selecting appropriate solid catalysts. This method can promote ozone decomposition, which will generate more reactive oxygen species (ROS) and further enhance the degradation of organic compounds (Peng et al., 2018; Zhang et al., 2020).

Metal oxides (e.g., MnO_2, Fe oxides, $CoFe_2O_4$, TiO_2) have been widely used as the catalysts in heterogeneous catalytic ozonation (Du et al., 2020; Liu et al., 2019; Oliveira et al., 2019; Yang et al., 2014). Among these metal oxides, MnO_2 showed the excellent catalytic performance on benzene series degradation due to its strong redox coples of Mn^{2+}/Mn^{3+} and Mn^{3+}/Mn^{4+} on the surface of catalysts, diverse and crystallographic structure (Niu et al., 2019; Zhang et al., 2020). MnO_2 has great structural flexibility and crystallographic polymorphs (e.g., α-, β-, γ-, and δ-MnO_2) because the basic structural MnO_6 units can be linked in different manners forming tunnels (Wang et al., 2016). α-MnO_2 has been extensively studied due to its structural characteristics and excellent activity for ozone decomposition and catalytic ozonation (Wang et al., 2015; Zhu et al., 2017). Moreover, recent studies have showed that metal doping can improve the catalytic performance by modifying α-MnO_2 structure. Wang et al. synthesized Zr^{4+} doped α-MnO_2 nanowires, and observed that Zr^{4+} ions originally occupied the positions belonging to elemental manganese in the crystal structure and resulted in a mutual action between Zr^{4+} ions and Mn^{3+} ions, thus improving the catalytic performance of α-MnO_2 (Wang et al., 2018). Uematsu et al. reported that the morphology of α-MnO_2 was

changed by doping with Mo^{6+}, leading to an increase in its specific surface area and the number of catalytically active surface positions, which in turn improved the catalytic performance of the catalyst (Uematsu et al., 2016).

As a kind of transition metal, Co has a strong Co^{2+}/Co^{3+} redox cycle which can also promote electron transfer and thus improve catalytic oxidation efficiency (Anfar et al., 2021). Lv et al. reported that Co doping on Fe_3O_4 increased the catalytic activity and stability of Fe_3O_4 (Lv et al., 2012). Li et al. observed that an interface synergistic effect between the doped metal Co and cerium oxide on catalyst Co-Ce-MCM-48 improved the interface electronic behavior and promoted the production of ROS (Li et al., 2019). Faleh et al. developed a new heterogeneous cobalt (Co) catalyst supported on activated carbon (Co/AC) and found the doping of Co improved the surface adsorption capacity of activated carbon which enhanced the degradation efficiency of oxalic acid in catalytic ozonation process (Faleh et al., 2019). Additionally, some studies have showed that the synergistic role can be well presented when the radius of doped metal ions is close to that of metal ions in the catalyst (Kang et al., 2013). Therefore, due to the close ionic radius between Co^{2+} and Mn^{2+}, the catalyst with Co doping on the α-MnO_2 might have a better catalytic activity than that of the sole α-MnO_2 catalyst. However, it is not clear how influence cobalt doping on its structure and physical and chemical properties.

In this article, α-MnO_2 catalyst doped with Co^{2+} was prepared by hydrothermal method, and then investigate the catalytic ozonation activities on phenol removal. BET, XRD, XPS and FTIR were used to analyze the phase, morphology and structural properties of the synthesized catalysts. The catalytic ozonation mechanism of Co-doped α-MnO_2 catalyst on phenol removal was explored in depth by the masking experiment of free radicals combining with catalyst structure characteristics.

2. Experimental

2.1 Materials and reagents

Potassium permanganate ($KMnO_4$, ≥99%), Manganese sulphate ($MnSO_4·H_2O$, ≥98%), Cobalt Sulfate ($CoSO_4·7H_2O$, ≥98%) were purchased from Sinopharm Chemical Reagent Co., Ltd. Deionized water was obtained from a Millipore Q water purification system. All reagents and chemicals were of analytical grade.

2.2 Synthesis of Catalysts

Co-doped α-MnO_2 were synthesized using a modified hydrothermal method, which was showed in Fig. 1. Co-doped α-MnO_2 were synthesized via a one-step hydrothermal method according to a previous report (Hu et al., 2020). 36 mmol of $MnSO_4·H_2O$ and certain molar of $CoSO_4·7H_2O$ were dissolved in 50 mL of deionized water under stirring, and then the above mixed solution was added into 50 mL Potassium homologate solution ($KMnO_4$ was 20 mmol) dropwise, followed by stirring magnetically for about 30 min until the solution became homogeneous. After that, it was transferred into a 200 mL Teflon-lined stainless-steel autoclave. The autoclave was kept at 160°C for 16 h in an oven and then cooled to room temperature, and then, the product was collected by filtration and fully rinsed several times with deionized water to remove K^+, followed by

drying at 105℃ for 8 h. In order to determine the optimal doping ratio, we prepared catalysts with different initial molar ratio of Co and Mn (0.1, 0.2, 0.3, 0.4 and 0.5 respectively). The sample with Co/Mn = 0.2 had the highest catalytic ozonation of phenol (Fig S1). Therefore, catalysts with Co/Mn = 0.2 named Co-α-MnO_2 was the materials synthesized. The synthetic procedures for α-MnO_2 was similar to that for Co-doped α-MnO_2 with the exception of adding $CoSO_4 \cdot 7H_2O$ to the initial solution.

2.3 Catalysts characterization

The catalyst was purged 5 h at 120 ℃ under nitrogen atmosphere protection and then determined the BET surface area and pore-size distribution on a Micromeritics ASAP2020 analyser when the sample was cooled. Powder X-ray diffraction (XRD) analysis was carried out on a Bruker D8 ADVANCE Phaser using Cu Ka radiation (k = 0.15418 nm) with a LYNXEYE detector at 40 kV and 30 mA. X-ray photoelectron spectroscopy (XPS) was performed with an ESCALAB250 system equipped with an Al Kα excitation source and operated at 15 kW and 1486.6 eV. Fourier transformed infrared (FTIR) analyses were carried out using a NicoletiS10 FT-IR plus spectrophotometer in a wavelength range of 4000-400 cm^{-1}.

2.4 Catalytic ozonation activities

In this study, phenol was selected as the aim pollutant because it is one of the most common industrial wastewater contaminates and would cause serious ecological and environmental problems (Saputra et al., 2017). The phenol degradated by catalytic ozonation was performed in a self-regulating quartz reaction with 1 L aqueous solution showed in Fig. 2. The concentration of ozone was adjusted via controlling the current and flow rate of the ozone generator and measured by ozone detector. When the ozone concentration was stable and then bubbled into the integrated adsorption-catalytic ozonation reactor to start the reaction. The pneumatic panel was adopted to ensure that gaseous ozone was completely mixed with aqueous solution. During the reaction, ozone concentration and flow rate were set at 3.0 mg/L and 3.0 L/min, respectively. The tail gas was absorbed by potassium iodide solution. 2 g catalyst was mixed with 1 L phenol wastewater (initial concentration was 400 mg/L; pH = 10; 293 ± 1 K) in the reaction system. The residual phenol concentration and COD concentration of water samples were measured to evaluate removal performance.

3. Results And Discussions

3.1 Catalytic degradation of phenol

The phenol removal investigated by adsorption, ozonation and catalytic ozonation are indicated in Fig. 3. It is clear to Fig out that the phenol removal efficiencies achieved by adsorption (showed in red and black line in Fig. 3) are all less than 5%. So, the contribution of catalyst adsorption on phenol removal could be neglectable. The phenol removal efficiencies during 40 min are in order of Co-α-MnO_2 (97.47%) > α-MnO_2 (81.01%) > single ozonation (58.55%). Phenol removals were also described with pseudo zero-order, first order and second order kinetics, and the kinetic models were expressed as Eq. (1), Eq. (2) and Eq. (3).

$C_0 - C_t = K_1 t$ (1)

$-\mathrm{Ln}(C_t/C_0) = K_1 t$ (2)

$1/C_t - 1/C_0 = K_2t$ (3)

Where K_1, K_2, K_3 are the pseudo zero-order, first-order and second-order rate constant, respectively (min^{-1}); t represents the reaction time; C_0 and C_t stand for the phenol concentration at 0 min and t min, respectively.

The reaction rate constants in different processes are showed in Table 1. The removal efficiency of catalytic ozonation on phenol well accords with the first-order reaction kinetics, while that of single ozonation accords with the zero-order reaction kinetics. Based on first-order kinetic fitting, Co-α-MnO_2 achieved the highest reaction rate constant for phenol removal (0.092 min^{-1}), which was 2.09 and 4 times higher than that in α-MnO_2 (0.044 min^{-1}) and O_3 (0.023 min^{-1}), respectively. It can be further verified that the doping of Co on α-MnO_2 efficiently improved the catalytic activities. The results might be attributed to the changes of catalyst construction, elementary composition and surface properties, et al., which will be detailly discussed in the following section.

Table 1
Parameters of Kinetic Fitting for the Removal Phenol

order	Zero-order		First-order		Second-order	
System	$K_1(min^{-1})$	R^2	$K_2(min^{-1})$	R^2	$K_3(min^{-1})$	R^2
O_3	6.172	0.996	0.023	0.987	8.862×10^{-5}	0.951
O_3/α-MnO_2	8.386	0.945	0.044	0.991	2.763×10^{-4}	0.936
O_3/Co-α-MnO_2	10.303	0.909	0.092	0.975	1.986×10^{-3}	0.708

3.2 Specific surface and pore size distribution

The calculated results of specific surface area and pore volume of α-MnO_2 and Co-α-MnO_2 are showed in Table 2. It can be seen that Co-α-MnO_2 catalyst has a bigger of specific surface area (79.496 m^2/g) and pore volume (0.0396 cm^3/g) than that of α-MnO_2 The specific surface area and pore volume are more, the better catalytic activity can be obtained. The reason is that the large specific surface area and pore volume can promote the mass transfer rate between solid-liquid-gas (Ghuge and Saroha 2018). So, catalytic activity of Co-α-MnO_2 is more great than that of α-MnO_2. N_2 adsorption-desorption isotherm showed that two kinds of catalysts belong to typically type (as showed in Fig. 4) (Zhai and Hao 2017), indicating that the interaction between catalysts and adsorbate is weak. The surface of the catalysts generally adsorbs small molecules such as H_2O molecules, which decomposed to generate hydroxyl radicals to promote the catalytic ozonation (Zhao et al., 2009).

3.3 Crystal phase

The XRD results of α-MnO_2 and Co-α-MnO_2 catalysts are showed in Fig. 5. All patterns of the prepared α-MnO_2 and Co-α-MnO_2 catalyst samples can be indexed to body-centered tetragonal, which are same as that of the standard α-MnO_2 (JCPDS NO.44-0141). There are no additional peaks in XRD patterns be identified after Co doping, which indicates that the crystal structure of the preparation of test samples was the same as

that of α-MnO_2. This shows that Co doping enters the MnO_2 skeleton structure by replacing Mn or is embedded in the pore structure of the catalyst tunnel, rather than existing on the catalyst surface in the form of cobalt oxide with similar ionic radius to CO^{2+} and Mn^{2+}. However, the Co doping on α-MnO_2 would cause the deformation of α-MnO_2 lattice, which make the grain diameter decrease and the parameters a, b and c increase (as showed in Table 2) and show a distortion in the lattice cell, thus further promotes the migration of adsorbed oxygen to decompose and oxidize organic matter (Yu et al., 2020; Peña et al., 2004).

Table 2
Specific surface area, pore volume, Lattice Parameters and Grain Diameters of α-MnO_2 and Co-α-MnO_2

Catalysts	Specific surface area(m^2/g)	Pore volume(cm^3/g)	Lattice parameter			Grain diameter
			a (Å)	b (Å)	c(Å)	(Å)
α-MnO_2	51.166	0.0250	9.7681	9.7681	2.8529	320
Co-α-MnO_2	79.496	0.0396	9.7822	9.7822	2.8534	287

3.4 Surface chemical compositions

In order to further investigate the elemental valence on the catalyst surface, Mn 2P, O1s and Co2p of both α-MnO_2 and Co-α-MnO_2 characterized by XPS were presented in Fig. 5(b), Fig. 5(c) and Fig. 5(d), respectively. Fig. 6(b) shows that the XPS spectrum of Mn 2p contains two main peaks at binding energies of 657.5 ± 7.5 and 642.5 ± 2.5eV, which could be attributed to $Mn2P_{1/2}$ and $Mn2p_{3/2}$. The binder energy of the peak at 641.6 eV, 642.5 eV and 643.4 eV are found in $Mn2p_{3/2}$, which can be attributed to Mn^{3+} and Mn^{4+} (Zhou et al., 2018; Li et al., 2018), respectively. As showed in Table 3, the relative content of Mn^{3+} of Co-α-MnO_2 increases from 8.42–41.16% and the ratio of Mn^{3+}/Mn^{4+} increases from 0.092 to 0.70 compared with α-MnO_2. According to the results of the Table 5, the main valence state of Co in the catalyst is Co^{3+}, which indicates that the doped Co^{2+} has a redox reaction in the catalyst preparation process, and promotes the increase of the ratio of Mn^{3+}/Mn^{4+} in Co-α-MnO_2. The higher ratio of Mn^{3+}/Mn^{4+} in Co-α-MnO_2 is an important reason for the occurrence of more oxygen vacancy, which would promote the generation of reactive oxygen species and facilitate the migration and transformation of oxygen species (Liu et al., 2019; Liu et al., 2009). In addition, Mn^{3+} and other unsaturated metal ions behave as Lewis acid in the aqueous phase, which is easy to coordinate with water molecules and undergo chemical adsorption to form the surface hydroxyl group. Furthermore, the XPS spectrums of O1s for α-MnO_2 and Co-α-MnO_2 are showed in Fig. 5(c). The binding energy energies at the peak position 530.1 eV and 531.5 eV in the O1s spectrum, corresponding to the lattice oxygen and the adsorbed oxygen respectively (Ge et al. 2017). Oxygen presenting form and relative content of oxygen calculated are showed in Table 4. Compared with α-MnO_2, the ratio of adsorbed oxygen (O_{ads})/ lattice oxygen (O_{latt}) of Co-α-MnO_2 increases from 0.15 to 0.23, indicating that more O_{latt} would combine with H_2O to produce surface hydroxyl, which is the active site for the catalyst to adsorb and decompose ozone to produce reactive oxygen, and then improve the efficiency of catalytic ozone oxidation. Surface hydroxyl group is well confirmed by the results of the following FT-IR analysis.

Table 3
Relative element content of α-MnO_2 and Co-α-MnO_2

Catalysts	Mn (%)	O (%)	Co (%)	Mn/O	Co/Mn	Co/O
α-MnO_2	27.77	56.59	-	0.491	-	-
Co-α-MnO_2	23.21	55.64	4.27	0.417	0.184	0.076

Table 4
XPS energy spectra analysis of α-MnO_2 and Co-α-MnO_2

Catalysts	Mn^{3+} (%)	Mn^{4+} (%)	Mn^{3+}/Mn^{4+}	Co^{2+}	Co^{3+}	Co^{2+}/Co^{3+}	O_{ads} (%)	O_{latt} (%)	O_{ads}/O_{latt}
α-MnO_2	8.42	91.58	0.092	-	-	-	13.32	86.68	0.15
Co-α-MnO_2	41.16	58.84	0.70	20.67	79.33	0.26	18.99	81.01	0.23

3.5 Surface functional groups properties

In order to expose the influence of doping Co on surface functional groups of α-MnO_2, the catalysts were characterized with FT-IR, and the results are present in Fig. 7. Although the position is slightly shifted, the intensities of stretching vibration of Mn-O and Mn-O-Mn bonds (467cm^{-1}, 524 cm^{-1} and 719 cm^{-1}) (Mishrap et al., 2016; Abdel-Latif et al., 2015) are greatly improved, which is caused by the microstructure regulation due to the doping of Co on α-MnO_2, and has been verified by the results of XRD. The characteristic peak of Mn-OH presents at the wavelength of 1042 cm^{-1}, which is constructed by adsorbing water molecules on the catalyst surface and shedding hydrogen ions (Han et al., 2010). Compared with the α-MnO_2, the peak intensity of Mn-OH in Co-α-MnO_2 increases obviously, indicating that the adsorption capacity of α-MnO_2 is improved by Co doping. The new peaks appeared at 879cm^{-1}, 1387cm^{-1} corresponding to the stretching vibration of Co-O (Fu et al., 2017), further confirm the XRD results of Co replacing Mn into the structure of α-MnO_2. The other three new peaks appeared at 1611cm^{-1}, 2969$cm^{-1}$and 3320cm^{-1} corresponded to the stretching vibration of the surface hydroxyl (O-H) (Kim et al., 2009), which are produced by flexural and telescopic vibration of adsorbed water on the catalyst surface. Therefore, in the Co-α-MnO_2 catalytic ozonation system, more surface hydroxyl were generated, and they were showed as acidic or alkaline groups through proton exchange with aqueous solution, which promotes electron transfer and produces reactive oxygen species contributing to higher catalytic ozonation efficiency (Maehida et al., 2000; Lu et al., 2016).

3.6 Mechanisms of catalytic ozonation

3.6.1 Surface hydroxylation and ROS

In order to further recognize the role of surface hydroxyl of the catalysts, HPO_4^{2-} was introduced and employed to occupy surface hydroxyl to deactivate the catalytic performance (Nawaz et al., 2015). The results of masking experiments were showed in Fig. 8. In comparison to the experiments without masking agent, the phenol removal rates were much decreased because HPO_4^{2-} was added to deactivate surface

hydroxyl of catalyst. The removal rate of phenol obtained by single ozonation, O_3/α-MnO_2 and O_3/Co-α-MnO_2 were 52.74%, 57.62% and 64.58%, respectively, which are reduced by 5.81%, 23.39% and 32.89%, respectively. So, surface hydroxyl played a key role in these catalytic ozonation systems.

The surface hydroxyl group might be the main active cite for catalyst to absorb and further decomposed ozone to produce •OH. •OH and $•O^{2-}$ were active free radicals produced in the process of catalytic ozonation, which played an important role in the degradation of organic compounds. Tert-butanol and p-benzoquinone were introduced and employed to occupy •OH and $•O^{2-}$ in O_3, O_3/α-MnO_2 and O_3/Co-α-MnO_2 systems, respectively. The results of masking experiments were showed in Fig. 9 and Fig. 10. After the addition of TBA or PBQ as masking agent, the removal rates of phenol decreased by 13.28%, 31.88%, 40.33% and 9.63%, 18.46% and 35.63%, respectively, which indicated that both •OH and $•O_2^-$ were active oxygen influencing the degradation of phenol by catalytic ozonation. The addition of the catalyst promotes the decomposition of O_3 to generate •OH and $•O^{2-}$, while the doping of Co enhanced the catalytic activity of the catalyst.

3.6.2 Analysis of the catalytic mechanism

The masking experiment results demonstrated that the presence of surface hydroxyl group and reactive oxygen species promoted the degradation efficiency of phenol. Therefore, the mechanism of catalytic ozonation of phenol by α-MnO_2 and Co-α-MnO_2 was analyzed from the surface of polyphase catalysis (as showed in Fig. 11).

According to the adsorption-desorption isotherm of the catalyst, the interaction between the adsorption material and the adsorption gas is relatively weak, indicating that the interaction between the catalyst and the adsorbent is relatively weak (as showed in Fig. 4). The surface of the catalyst generally absorbs small molecules, so H_2O molecules are preferentially adsorbed than O_3 molecules (Zhao et al., 2009(a)). When introduced into an aqueous solution, H_2O molecules will be strongly adsorbed on the surface of catalyst. The adsorbed H_2O molecules will always dissociate into OH^- and H^+ (Zhao et al., 2009(a)), and form the surface hydroxyl group with the surface cation and oxygen anion respectively. The released HO_3• will further decompose and release O_2 and produce •OH. Then, the doping of Co could promote the generation of more surface hydroxyl groups, which promoted the catalytic ozonation process.

The surface hydroxyl group reacts with O_3 to form a surface five-member ring, which will further decompose to release O_2 and form surface HO_2^-. Surface HO_2^- on the one hand reacts further with O_3 to form HO_3^-, then releases O_2 to form •OH, and produces O_3^- at the same time. On the other hand, HO_2^- can further produce $•O_2^-$ by releasing H^+. Under the action of O_3 molecule, the surface $•O_2^-$ will form the surface cation, and the surface cation will absorb H_2O molecule to form the surface hydration cation (H_2O^+). With the release of HO_3^-, the •OH will be generated, while the surface H_2O^+ will be converted to the surface hydroxyl group (Zhao et al., 2009(b); Wang et al., 2016; Zhu et al., 2017). Therefore, the catalyst completed the surface hydroxyl regeneration and initiated the free radical chain reaction.

4. Conclusion

Co-doped α-MnO_2 was prepared by hydrothermal method to be as the catalyst for phenol removal. The removal performance and mechanism by catalytic ozonation was obtained. The results showed that Co doping played a great role in promoting the efficiency of phenol removal by catalytic ozonation over Co-α-MnO_2. After 40 min catalytic ozonation, the phenol removal rates by Co-α-MnO_2 reached 97.47%, which was 16.46%, 38.92% higher than that of α-MnO_2 catalytic ozonation and pure O_3 without catalyst respectively. The kinetic rate of Co-α-MnO_2 on phenol ozonation reaching 0.092min^{-1}, which was 2.09 times and 4 times of α-MnO_2 and ozonation without catalyst respectively. The higher catalytic activity of Co-α-MnO_2 catalyst could be attributed to a series of better properties in comparison with α-MnO_2 catalyst. Compared with α-MnO_2, the doping of Co made Co-α-MnO_2 had much larger specific surface area and pore volume, more crystal defect and oxygen vacancy, higher relative content of Mn^{3+} and adsorbed oxygen (O_{ads}) and more surface hydroxyl. The combined action of these factors finally improved the catalytic ozonation performance of Co-α-MnO_2. Masking experiments had showed that surface hydroxyl group and active free radicals (·OH and $·O^{2-}$) were involved in the catalytic ozonation of phenol. Furthermore, the primary reaction mechanism was proposed. The catalyst achieved the regeneration of surface hydroxyl group and the initiation of free radical chain reaction. The doping of Co promoted these reactions by producing more surface hydroxyl groups, which promoted the catalytic ozonation process.

Declarations

Acknowledgements

Thanks for the Fundamental Research Funds for the Central Universities (2019XKQYMS78), the Open Sharing Fund for the Large-scale Instruments and Equipments of China University of Mining and Technology (CUMT) and Postgraduate Research & Practice Innovation Program of Jiangsu Province (SJCX21_1020)'s support.

Funding

This work was supported by the Fundamental Research Funds for the Central Universities (2019XKQYMS78).

Competing Interests

The authors have no relevant financial or non-financial interests to disclose.

Author Contributions

D.B. (M.D. student), Z.X.C. (M.D. student) and H.Y. (M.D. student) conducted all the experiments and wrote the manuscript. Z.J. (Associate Professor) and H.S.L. (Professor) wrote and revised the manuscript. G.S.J. (Associate Professor) peformed data analysis and interpretation as well as revised the manuscript.

Ethical Approval

Not applicable

Consent to Participate

Not applicable

Consent to Publish

Not applicable

References

1. Abdel-Latif IA, Ismail AA, Bouzid H, Al-Hajry A (2015) Synthesis of novel perovskite crystal structure phase of strontium doped rare earth mangantites using solgel method. J Magn Magn Mater 393: 233-238.
2. Anfar Z, Fakir AAE, Zbair M (2021) New functionalization approach synthesis of Sulfur doped, Nitrogen doped and Co-doped porous carbon: Superior metal-free Carbocatalyst for the catalytic oxidation of aqueous organics pollutants. Chem Eng J 405: 126660.
3. Chen CM, Li Y, Ma WF, Guo SH, Wang QH, Li QX (2017) Mn-Fe-Mg-Ce Loaded Al_2O_3 Catalyzed Ozonation for Mineralisation of Refractory Organic Chemicals in Petroleum Refinery Wastewater. Sep Purif Technol 183: 1-10.
4. Du Jk, Xiao GF, Xi YX, Zhu XW, Su F, Sang. HK (2020) Periodate Activation with Manganese Oxides for Sulfanilamide Degradation. Water Res 169: 115278.
5. Fu Y, Yun D, Tang JJ, Zhou SH, Wang BB (2017) Oriented surface decoration of (Co-Mn) bimetal oxides on nanospherical porous silica and synergetic effect in biomass-derived 5-hydroxymethyl furfural oxidation. Mol Catal 435: 144-155.
6. Faleh S, Guiza M, Quederni A (2019) An Optimization Study of Cobalt Supported on Activated Carbon for the Catalytic Ozonation of Oxalic Acid: Effect of Operating Parameters and Synergetic Combination. Ozone-Sci Eng 41(3): 274-285.
7. Ge G, Shi JW, Chang L et al (2017) Mn/CeO_2 catalysts for SCR of NOx with NH_3: comparative study on the effect of supports on low-temperature catalytic activity. Appl Surf Sci 411: 338-346.
8. Ghuge SP, Saroha AK (2018) Catalytic ozonation of dye industry effluent using mesoporous bimetallic Ru-Cu/SBA-15 catalyst. Process Saf Environ 118, 125-132.
9. Han N, Wu XF, Chai LY, Liu HD, Chen YF (2010) Counterintuitive sensing mechanism of ZnO nanoparticle based gas sensors. Sensors Actuat B Chem 150(1): 230-238.
10. Hu L, Xia Z (2018) Application of Ozone Micro-Nano-Bubbles to Groundwater Remediation. J Hazard Mater 342**:** 446-453.
11. Hu XL, Chen JX, Li SY, Chen YX, Qu WY (2020) The Promotional Effect of Copper in Catalytic Oxidation by Cu-Doped α-MnO_2 Nanorods. Phy Chem 124: 701-708.
12. Kim YJ, Taniguchi Y, Murase K, Taguchi Y, Sugimura H (2009) Vacuum ultraviolet-induced surface modification of cyclo-olefin polymer substrates for photochemical activation bonding. Appl Surf Sci 255(6): 3648-3654.

13. Kang JL, Hirata A, Kang LJ, Zhang XM, Hou Y (2013) Enhanced supercapacitor performance of MnO by atomic doping.Angew Chem Int Edit 125(6): 1708-1711.
14. Liu FD, He H, Ding Y, Zhang CB (2009) Effect of manganese substitution on the structure and activity of iron titanate catalyst for the selective catalytic reduction of NO with NH_3. Appl Catal B Environ 93(1): 194-204.
15. Lv AH, Hu C, Nie YL, Qu JH (2012) Catalytic ozonation of toxic pollutants over magnetic cobalt-doped Fe_3O_4 suspensions. Appl Catal B Environ 117: 246-252.
16. Lu J, Wei X, Chang Y, Tian SG, Xiong Y (2016) Role of Mg in mesoporous $MgFe_2O_4$ for efficient catalytic ozonation of Acid Orange II. J Chem Technol Biotechnol 91(4): 985-993.
17. Li YF, Liu ZP (2018) Active Site Revealed for Water Oxidation on Electrochemically Induced δ-MnO_2: Role of Spinel-to-Layer Phase Transition. J Am Chem Soc 140(5): 1783-1792.
18. Li SY, Li XK, Wu HT, Sun XL, Gu FL (2019) Mechanism of Synergistic Effect on Electron Transfer over Co–Ce/MCM-48 during Ozonation of Pharmaceuticals in Water. Acs Appl Mater Inter 11: 23957-23971.
19. Liu Y, Wang JL (2019) Reduction of nitrate by zero valent iron (ZVI)-based materials: A review. Sci Total Environ 671: 388-403.
20. Liu D, Wang CR, Song YF, Wei YH, He L (2019) Effective mineralization of quinoline and bio-treated coking wastewater by catalytic ozonation using $CuFe_2O_4$/Sepiolite catalyst: Efficiency and mechanism. Chem 227: 647-656.
21. Maehida M, Uto M, Kurogi D, Kijima T (2000) Mn-CeO_2 binary oxides for catalytic NO_x sorption at low temperature Sorptive removal of NO_x. Chem Mater 12: 3158-3164.
22. Mishrap J. Electrochemical depositon of MWCNT-MnO_2/PPynano-composite application for microbialfuelcells. Inte J Hydrogen Ene 41: 22394.
23. Nawaz F, Xie YB, Cao HB (2015) Catalytic ozonation of 4-nitrophenol over an mesoporous -MnO_2 with resistance to leaching. Catal Today 258(2): 595-601.
24. Niu Z, Yue T, Hu WJH, Sun W, Hu YH, Xu ZH (2019) Covalent bonding of MnO_2 onto graphene aerogel forwards: Efficiently catalytic degradation of organic wastewater. Appl Sur Sci 496: 143585.
25. Oliveira JSD, Salla JDS, Kuhn RC, Jahn SL, Foletto EL (2019) Catalytic Ozonation of Melanoidin in Aqueous Solution over $CoFe_2O_4$ Catalyst. Mater Res. 22: e20180405.
26. Peña DA, Uphade BS, Smirniotis PG (2004) TiO_2-supported metal oxide catalysts for low-temperature selective catalytic reduction of NO with NH_3: I. Evaluation and characterization of first row transition metals. J Catal 221(2): 421-431.
27. Peng JL, Lai LD, Jiang X, Jiang WJ, Lai B (2018) Catalytic Ozonation of Succinic Acid in Aqueous Solution using the Catalyst of Ni/Al_2O_3 Prepared by Electroless Plating-calcination Method. Sep Purif Technol 195: 138-148.
28. Saputra E, Duan XG, Pinem JA, Bahri S, Wang SB (2017) Shape-controlled Co_3O_4 catalysts for advanced oxidation of phenolic contaminants in aqueous solutions. *Separation and Pur Technol* 186.

29. Uematsu T, Miyamoto Y, Ogasawara Y, Suzuki K, Yamaguchi K, Mizuno N (2016) Molybdenum-Doped α-MnO_2 as an Efficient Reusable Heterogeneous Catalyst for Aerobic Sulfide Oxygenation. Catal Sci Technol 6, 222-233.
30. Wang C, Ma JZ, Liu FD, He H, Zhang RD (2015) The Effects of Mn^{2+} Precursors on the Structure and Ozone Decomposition Activity of Cryptomelane-Type Manganese Oxide (OMS-2) Catalysts. J Phys Chem C 119(40): 23119-23126.
31. Wang L, He H, Zhang CB, Sun L, Liu SJ, Wang SX (2016) Antimicrobial activity of silver loaded MnO_2 nanomaterials with different crystal phases against Escherichia coli. J Environ Sci 41(3): 112-120.
32. Wang Y, Yang WZ, Yin XS, Liu Y (2016) The role of Mn-doping for catalytic ozonation of phenol using Mn/γ-Al_2O_3 nanocatalyst: Performance and mechanism. J Environ Chem Eng 4: 3415-3425.
33. Wang YC, Li YZ, Lu ZG,Wang W (2016) Improvement of O_2 adsorption for α-MnO_2 as an oxygen reduction catalyst by Zr^{4+} doping. Rsc Advances 8(6): 2963-2970.
34. Wang J, Chen H (2020) Catalytic Ozonation for Water and Wastewater Treatment: Recent Advances and Perspective. Sci Total Environ 704: 135249.6.
35. Yang Y, Cao H, Peng P, Bo H (2014) Degradation and transformation of atrazine under catalyzed ozonation process with TiO_2 as catalyst. J hazard mater 279: 444-451.
36. Yu YL, Li CT, Du XY, Zhu YC, Zhang YD, Li SH (2020) Catalytic oxidation of toluene over MnO_2 catalysts with different Mn (II) precursors and the study of reaction pathway. Fuel 262: 116610.
37. Zhao L, Ma J, Sun ZZ (2009(a)) Mechanism of heterogeneous catalytic ozonation of nitrobenzene in aqueous solution with modified ceramic honeycomb. Appl Catal B 89: 326-334.
38. Zhao L, Sun ZZ, Ma J (2009(b)) Novel Relationship between Hydroxyl Radical Initiation and Surface Group of Ceramic Honeycomb Supported Metals for the Catalytic Ozonation of Nitrobenzene in Aqueous Solution. *Environm Sci Technol* 43(5): 4157-4163.
39. Zhu GX, Zhu JG, Jiang WJ, Zhang ZJ, Wang J (2017) Surface oxygen vacancy induced α-MnO_2 nanofiber for highly efficient ozone elimination. Appl Cataly B Environ 209: 729–737.
40. Zhai HY, Hao Z (2017) Synthesis of Cr, Ag Co-Doped ZnS Nanomaterials and Its Adsorption Capability for Reactive Dyes. *Spectroscopy & Spectral Analysis* 37(08): 2638-2644.
41. Zhu GX, Zhu JG, Jiang WJ, Zhan ZJ, Wang J, Zhu YF, Zhang QF (2017) Surface oxygen vacancy induced α-MnO_2 nanofiber for highly efficient ozone elimination. Appl Cataly B: Environ 209(3): 729-737.
42. Zhou CS, Wang J, Liu X, Chen FY, Di YY (2018) Magnetic and thermodynamic properties of α, β, γ and δ-MnO_2. New J Chem 42(10): 8400-8407.
43. Zhang JL, Xiong ZK, Wei J (2020) Catalytic Ozonation of Penicillin G using Cerium-loaded Natural Zeolite (CZ): Efficacy, Mechanisms, Pathways and Toxicity Assessment. Chem Eng J 383: 123144.
44. Zhang J, Dong B, Ding D, He SL, Ge SJ (2021) Removal Efficiency and Mechanism of Bio-treated Coking Wastewater by Catalytic Ozonation Using MnO_2 Catalyst Modified with Anionic Precursors. Environ Eng Res 26(5): 200394.

Figures

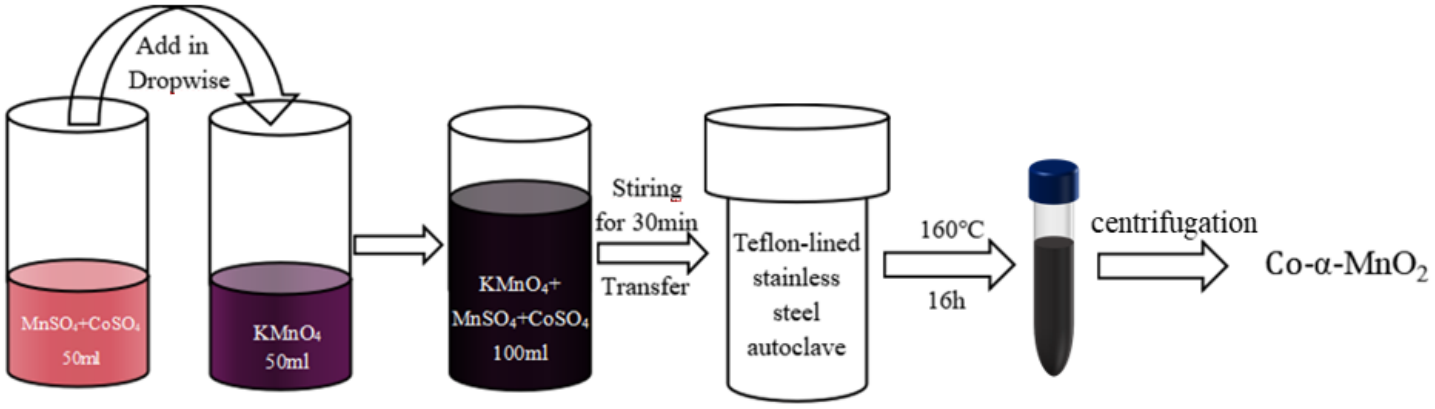

Figure 1

Preparation flowchart of a new Co-doped α-MnO_2 as catalyst.

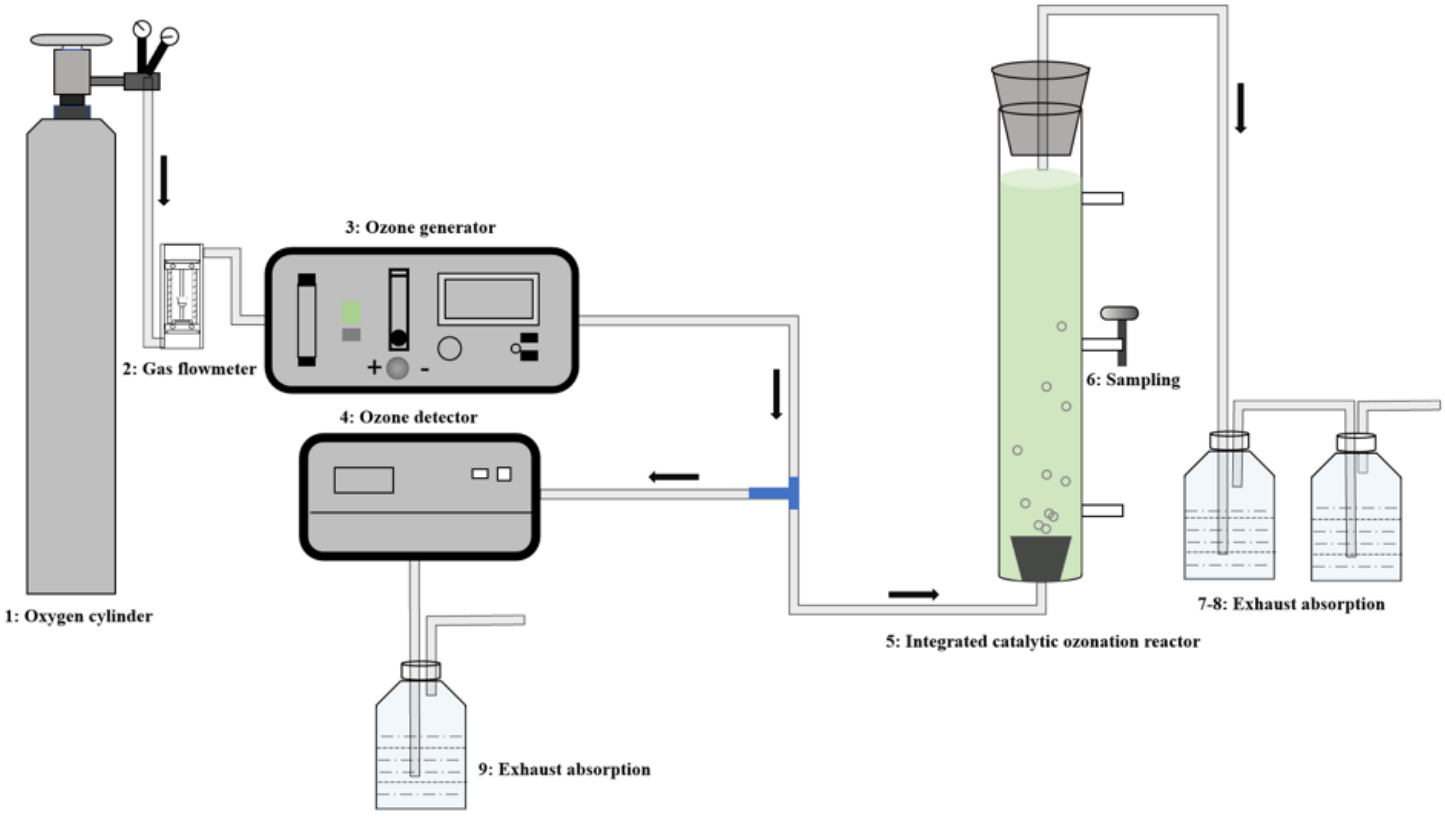

Figure 2

Experimental Installation.

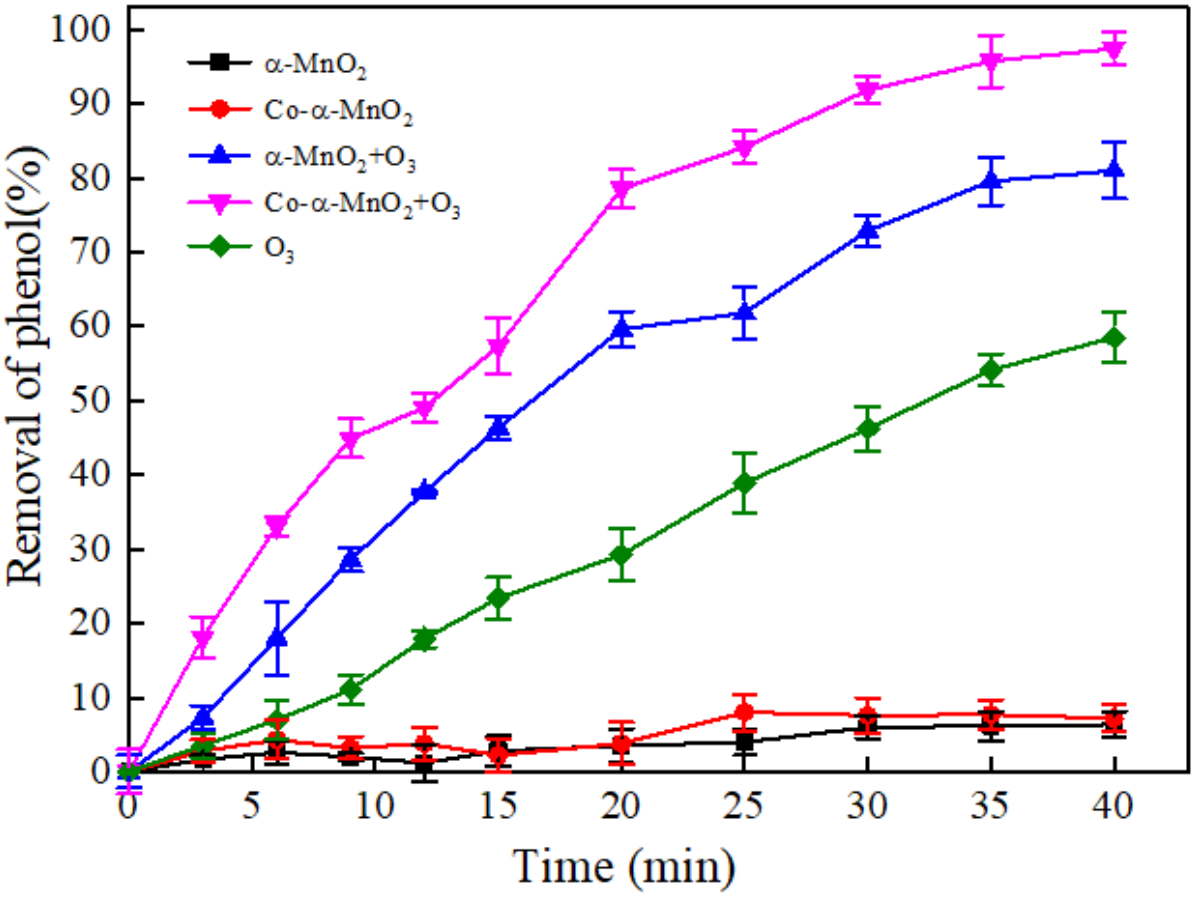

Figure 3

Comparison of the degradation efficiency of phenol in the different processes.

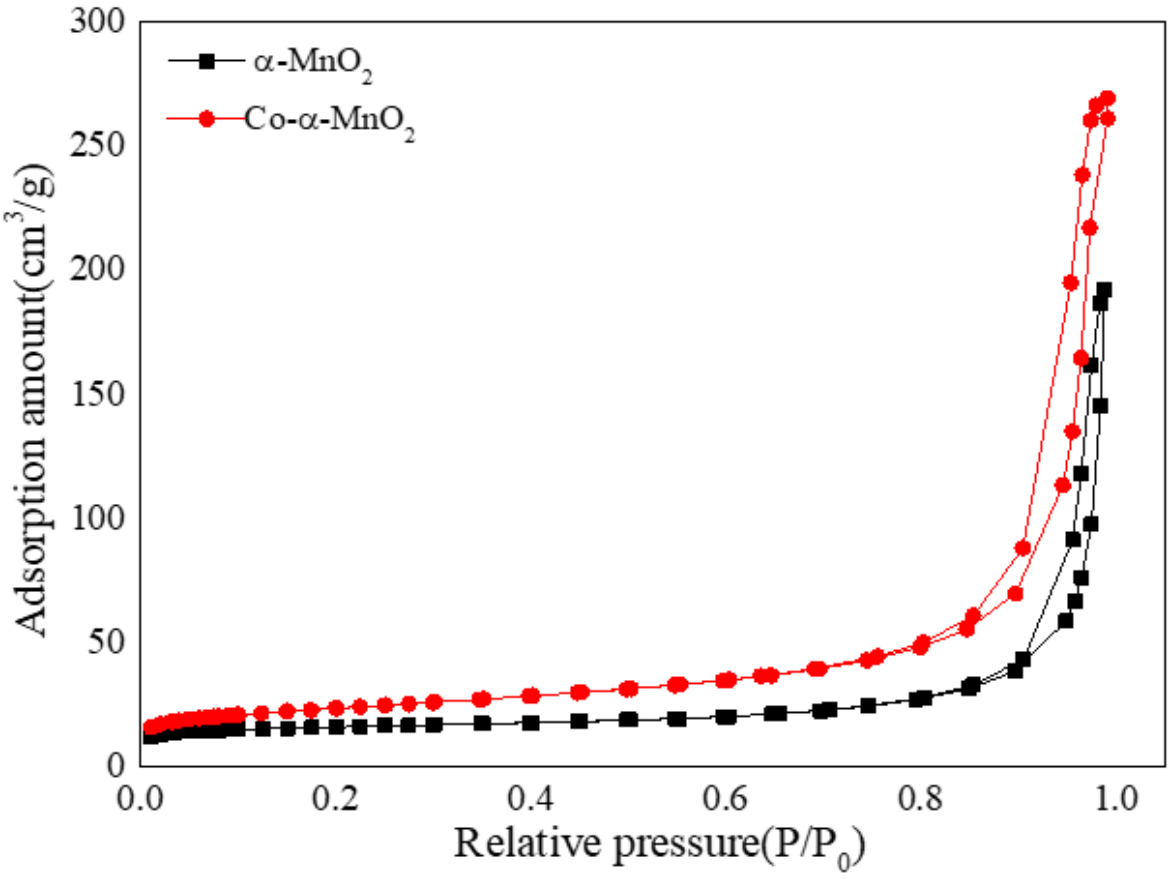

Figure 4

N_2 adsorption-desorption isotherms of α-MnO_2 and Co-α-MnO_2

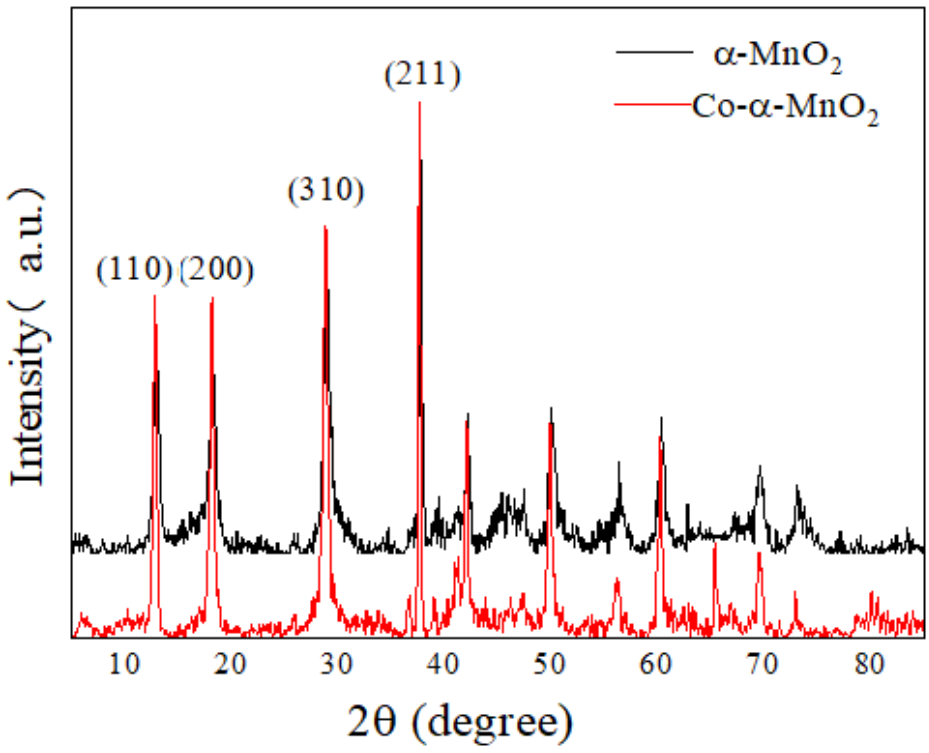

Figure 5

XRD patterns of α-MnO_2 and Co-α-MnO_2

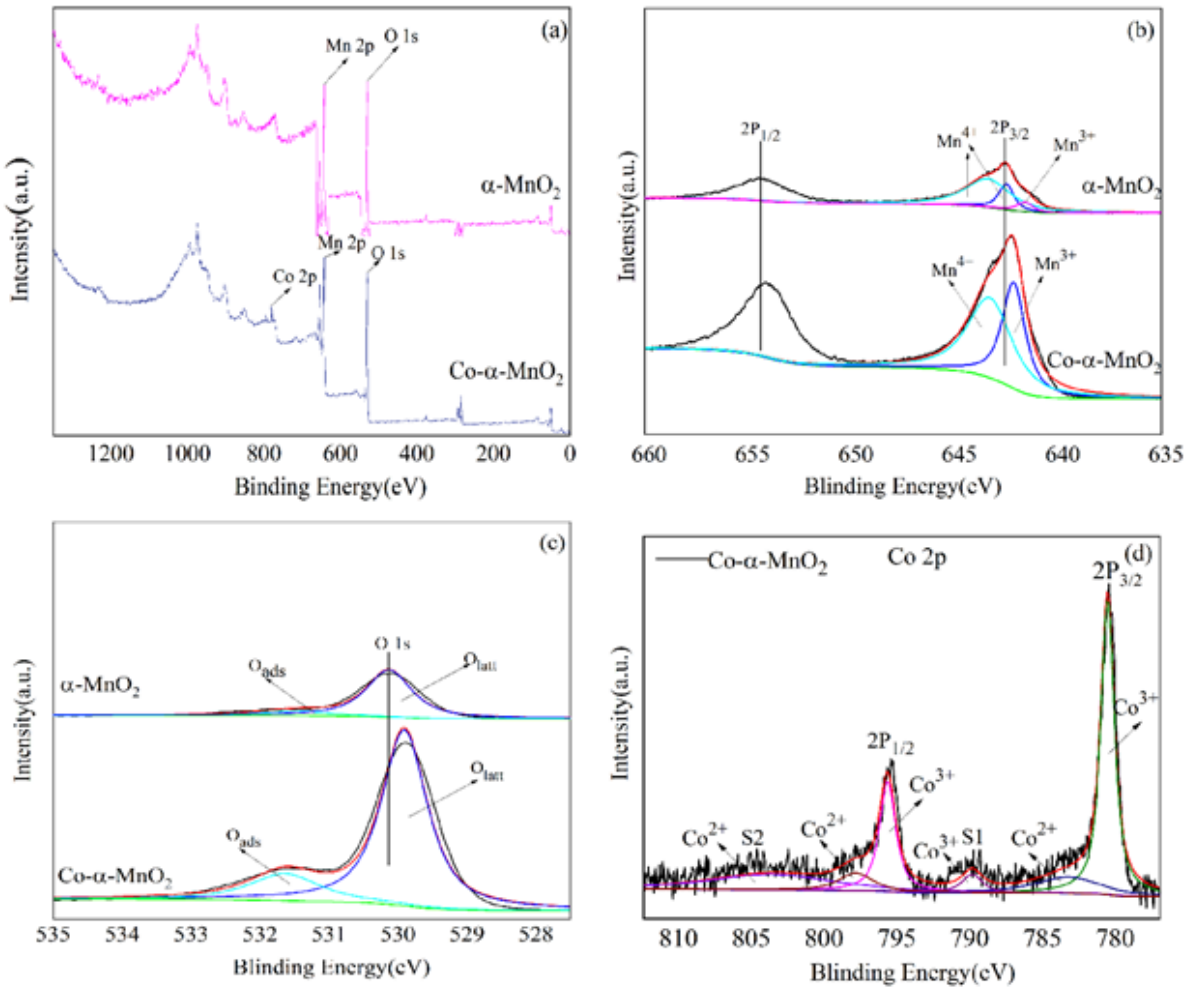

Figure 6

XPS spectrums of α-MnO_2 and Co-α-MnO_2: (a) Full spectrums; (b) Mn2P; (c) O1s; (d) Co2p

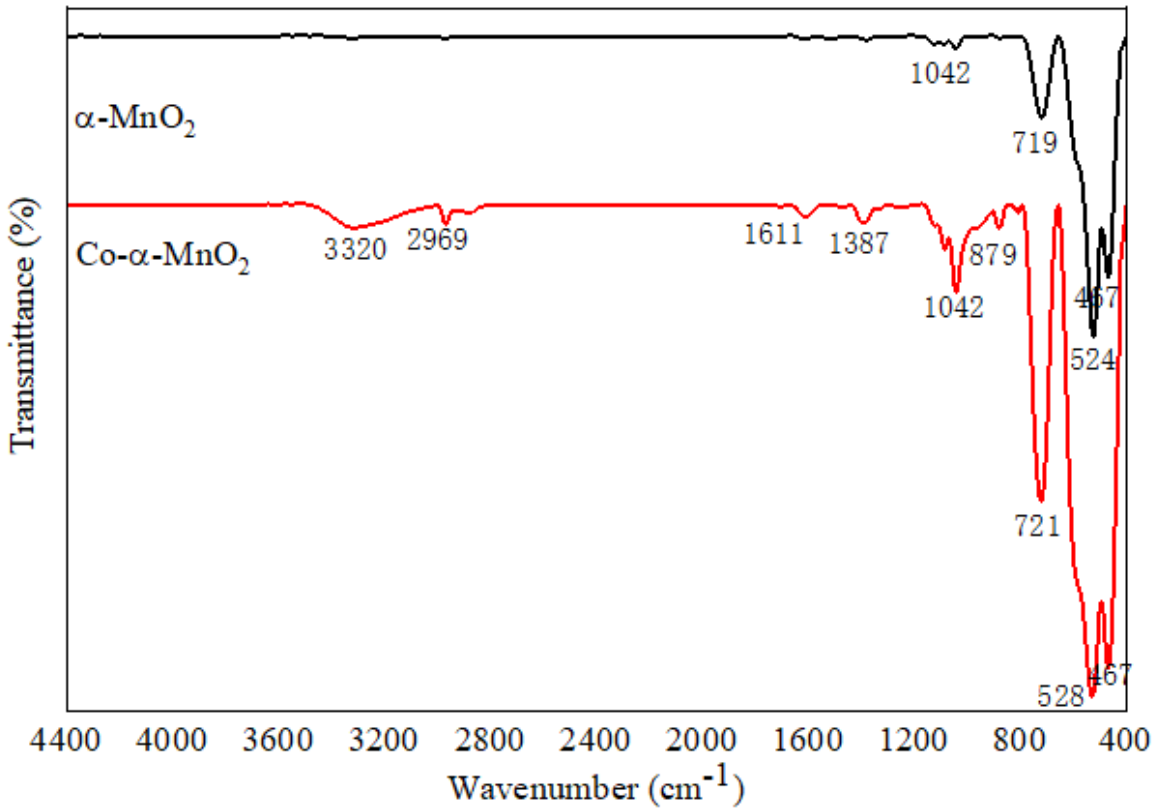

Figure 7

Infrared spectra of α-MnO_2 and Co-α-MnO_2

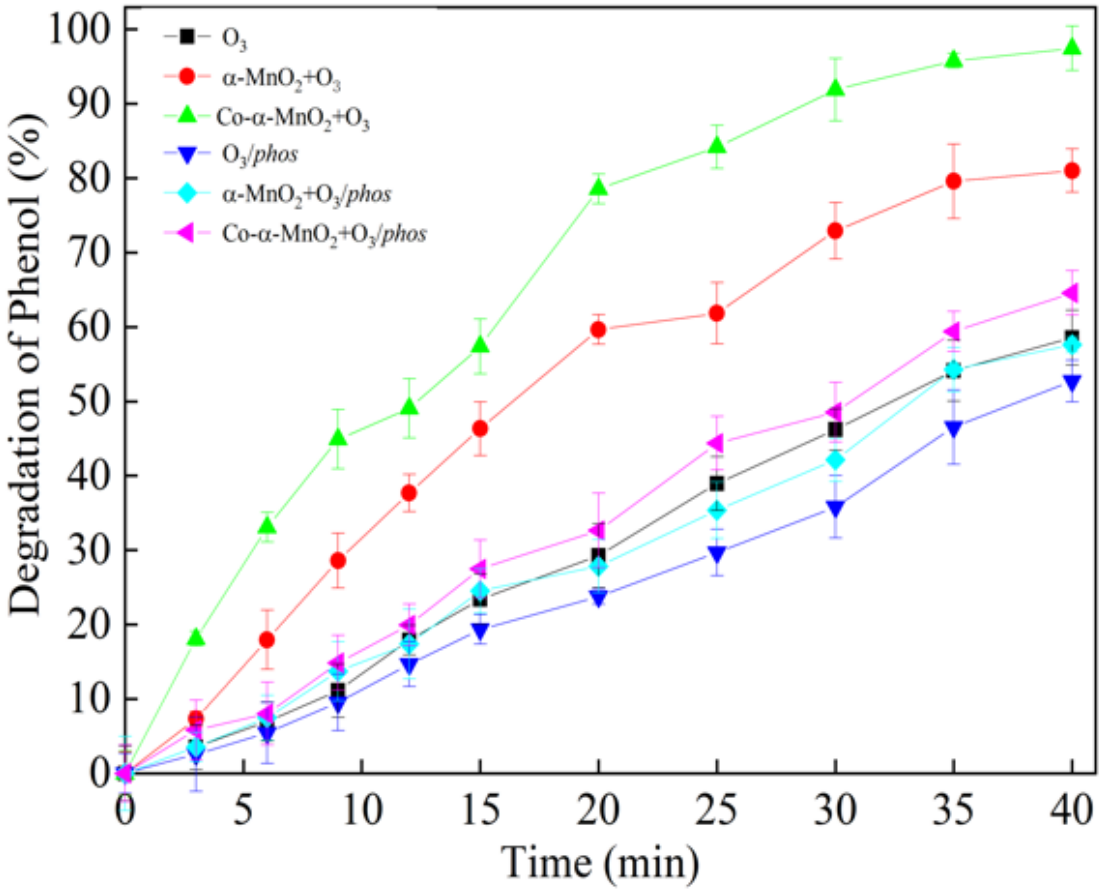

Figure 8

Effect of phosphates on phenol degradation

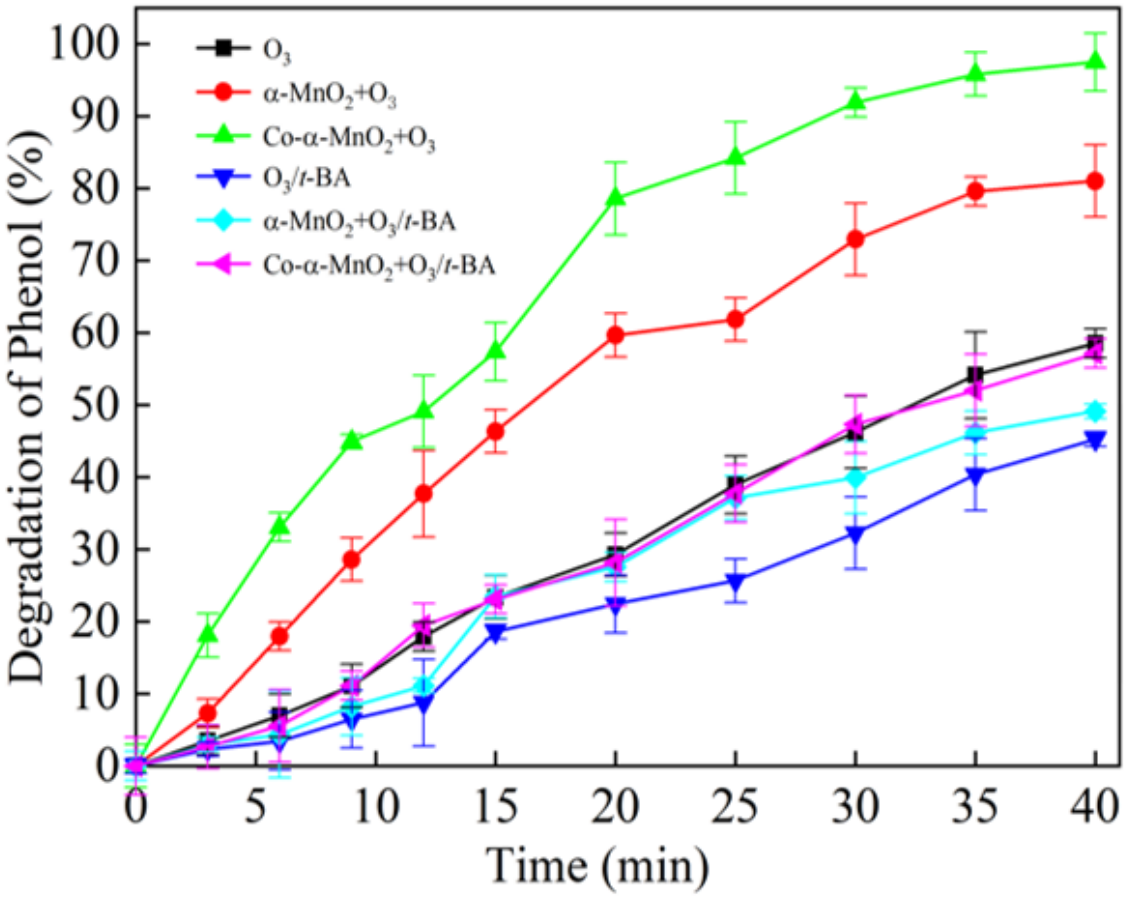

Figure 9

Effect of TBA on phenol degradation

Figure 10

Effect of PBQ on phenol degradation

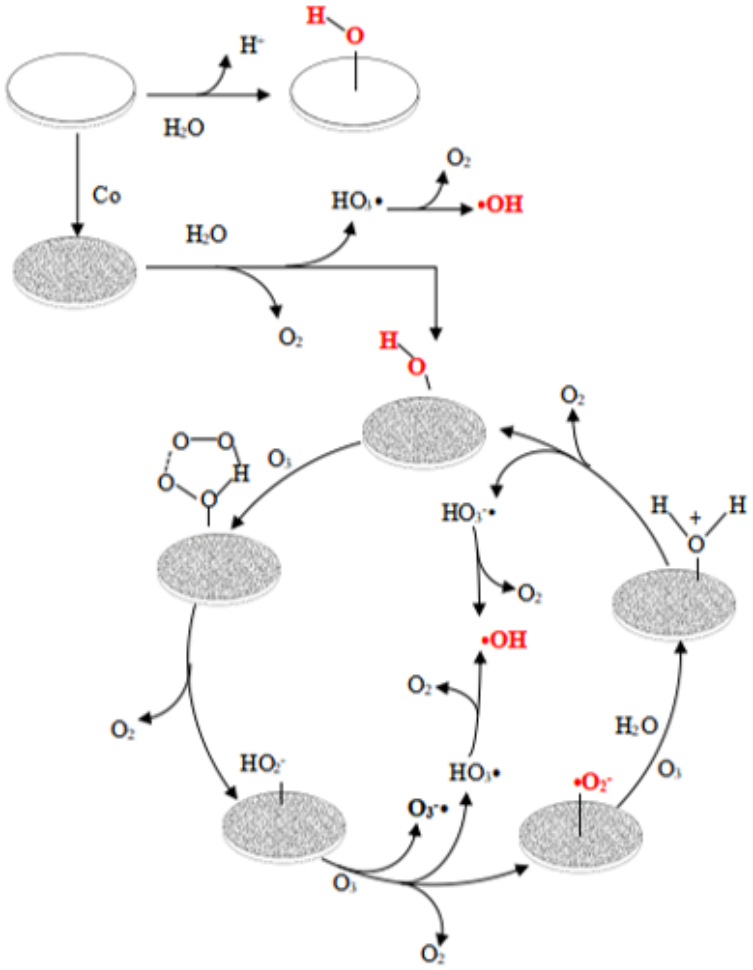

Figure 11

Mechanism of phenol degradation by catalyst

Supplementary Files

This is a list of supplementary files associated with this preprint. Click to download.

- SupplmentaryMaterial.docx